Broadband Control of Topological Nodes in Electromagnetic Fields

Alex Y. Song, Peter B. Catrysse, and Shanhui Fan

Broadband Control of Topological Nodes in Electromagnetic Fields

Alex Y. Song, Peter B. Catrysse, and Shanhui Fan*

Department of Electrical Engineering, Stanford University, Stanford, CA94305

We study topological nodes (phase singularities) in electromagnetic wave interactions with structures. We show that, when the nodes exist, it is possible to bind certain nodes to a specific plane in the structure by a combination of mirror and time-reversal symmetry. Such binding does not rely on any resonances in the structure. As a result, the nodes persist on the plane over a wide wavelength range. As an implication of such broadband binding, we demonstrate that the topological nodes can be used for hiding of metallic objects over a broad wavelength range.

Keywords: Electromagnetic Waves, Topological Nodes, Broadband Hiding

A topological node in electromagnetic fields, also known as a phase singularity, can appear along the axis of wave propagation (i.e. as in an optical vortex beam), or transverse to the axis [1–3]. The former case has drawn significant recent interest due to potential applications such as in optical communication or small particle manipulation [4–11]. Several aspects of the topological nodes in the transverse scenario have also been studied before. Examples include their statistics in random wavefields, and their general topological structure [12–16].

In the transverse scenario, since the electromagnetic field vanishes at the topological node, it is natural to think of using the nodes for "hiding" purposes. A small object placed on these nodes will have minimal interaction with the electromagnetic fields, and therefore is hidden from the field. For this purpose then, it would be important to understand the mechanisms that control the location of these nodes. Moreover, it is of interest to design structures in which the location of nodes does not vary much under change of frequency, since one can then perform broadband electromagnetic hiding, i.e. to ensure that the object located at certain positions is invisible even to broadband incident electromagnetic waves.

In this paper, we show that it is possible to bind the location of the nodes to a symmetry plane over a broad wavelength range. The structure under consideration is a photonic crystal slab under plane wave incidence. The nodes exist in a wide wavelength range away from the guided resonances. The restriction of the nodes' location is enforced by the mirror symmetry in the structure and the time-reversal symmetry, and does not rely on any resonances in the materials or the structure. The binding occurs despite the fact that the field itself does not share the full symmetry of the structure, since the wave is only incident from one side. As an implication of the broadband binding, we demonstrate that it is possible to use the nodes to hide objects over a broad wavelength range.

The generic structure is a photonic crystal slab with a periodic permittivity in the x direction as

$$\varepsilon = \begin{cases} \varepsilon_0 \varepsilon_r(x), & -d/2 \leq z \leq d/2 \\ \varepsilon_0, & elsewhere \end{cases} \tag{1}$$

where ε_0 is the vacuum permittivity, $\varepsilon_r(x) = \varepsilon_r(x + L)$, and L is the period length. The layer is uniform in y. A simple example of such a structure is an array of rectangular dielectric objects in vacuum, shown in Fig. 1a. We assume s-polarized plane wave (electric field in y-direction) incidence from $-z$ side. The field distribution in the structure can be solved by rigorous coupled wave analysis (RCWA) [17–19]. The electric field intensity distribution at several wavelengths in the non-diffracting regime (i.e. periodicity smaller than the free space wavelength) are shown in Fig. 1c-g. The transmission spectrum of this structure is plotted in Fig. 1b as a reference. The existence of a node is most evident in the phasor diagram, where the real and the imaginary parts of the electric field amplitude are represented by the x- and y-components of the phasor vectors, respectively. The phasor diagram is also shown in Fig. 1c-g. We emphasize that in this configuration the electric field is a complex scalar, and the phasor vectors are not vectors in the physical space. Inside the regions marked by the red arrows in Fig. 1d, e, and g, the phasor diagrams show a vortex shape. Mathematically, the phasor diagram is a smooth vector field $\nu : \mathcal{M} \to R^2$, i.e. a map from the manifold $\mathcal{M}$ of the x-y plane to R^2 [20]. A node in ν is characterized by its Poincaré index [1, 21], which is an integer invariant defined as the degree of mapping $\nu/|\nu| : \mathcal{D} \to S^1$, where $\mathcal{D}$ is an arbitrarily shaped loop enclosing the node, and S^1 is the unit circle. A non-zero degree of mapping, e.g. as in a vortex, guarantees the existence of a node. In Fig. 1d, e, and g we have marked the indices of the nodes accordingly. Similar arguments, carried out in the wavevector space, have been previously used to characterize the topological properties of bound states in continuum [22]. Here we apply this argument in real space.

In this fairly simple dielectric structure, the topological nodes nevertheless exhibit several remarkable features: (1) the nodes always show up in pairs, and their indices sum to zero. (2) The nodes persist over a wide range of wavelengths despite the drastically different overall field distribution, for example at the wavelengths of 2.5, 2.0 and 1.25 L shown in Fig. 1. Most importantly, these nodes are in fact confined exactly on the $z = 0$ mirror
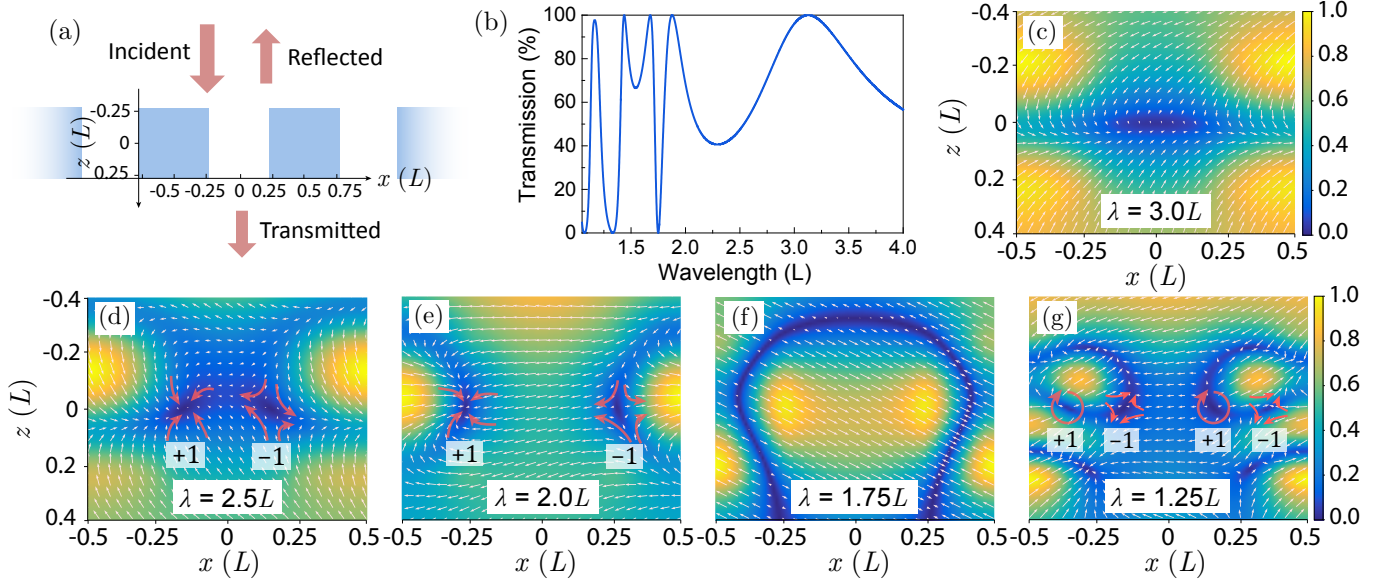
Figure 1. (a) A periodic array of dielectric objects (blue) under plane wave incidence. (b) The transmission spectrum of the structure in the wavelength range of 1.1-4.0 L, where L is the period length. (c)-(g) Field distributions at the wavelengths of 3.0, 2.5, 2.0, 1.75 and 1.25 L. The pseudo-color plot represent the electric field intensity (a.u.). The vectors represent the phasor diagram. The red arrows indicate the direction of vector flow around a node. The indices of the nodes are marked. The dielectric box has a size of $0.55 \times 0.55\,L$ with a permittivity of $\varepsilon_1 = 12$.

plane, even though the field itself is not mirror symmetric with respect to the $z = 0$ plane. (3) The nodes may disappear when a nodal line appears, e.g. in Fig. 1f, or when they annihilate with each other, e.g. in Fig. 1c for wavelengths above $3\,L$. In the following, we account for these features with topological arguments and a microscopic model based on time-reversal and mirror symmetries.
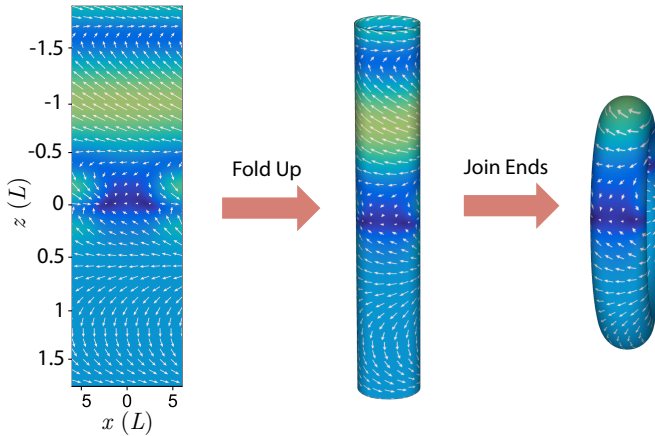

Figure 2. A demonstration of the gluing procedure. Left: the field distribution in one period of the structure at the wavelength of $2.5\,L$. Middle: the field plot is fold up and glued along the two x-boundaries, forming a cylinder. Right: the cylinder is bent and glued along the two ends, forming a torus T^2.

The observation that the nodes show up in pairs in a

period can be understood as a result of the mirror symmetry at $x = 0$, since the mirror image of a node is also a node with the opposite index [23]. However, there is a stronger global topological argument that guarantees this observation, which does not require the mirror symmetry. To show this, we resort to a common technique in differential topology, namely gluing [24]. Gluing requires the vector field along the boundaries to be smooth and continuous. The structure here has periodic boundary condition in the x direction, which satisfies the requirement. Thus, we can roll up a period and glue its two edges to form a cylinder, as is illustrated in Fig. 2. The structure is not periodic in z. However, the dynamics of the phasor vectors in the regions sufficiently far away from the dielectric structure is known. In the nondiffracting regime, the electromagnetic field asymptotically approaches plane waves far away from the grating layer. A plane wave does not contain any node. Therefore, the vector field ν has no node in the $z \gg 0.5\,L$ and $z \ll -0.5\,L$ regions in Fig. 2. Moreover, same as in a plane wave, ν rotates with varying z but remains constant for different x. Thus, we can always find an upper and lower boundary where ν points in the same direction. With that, we can bend the cylinder and glue its two ends to form a torus T^2. The magnitude of ν at the two ends may not always be equal, but in that case we can simply gradually tune the magnitude of ν along z till they match on the edge. This process is allowed since it would not change the existence or the index of any node [20]. After the gluing process, ν becomes a smooth vec-

tor field on T^2. Now, the Poincaré-Hopf theorem [25, 26] states that, for a vector field ν on a Manifold $\mathcal{M}$ pointing at the outward norm at ∂M, we have:

$$\sum_m \eta_m(\nu) = \chi(\mathcal{M}) \tag{2}$$

where m represent the nodes, η is the corresponding index, and $\chi(\mathcal{M})$ is the Euler characteristics of the manifold $\mathcal{M}$, which is a global invariant determined by the intrinsic topology of $\mathcal{M}$. A torus has no boundary, and $\chi(T^2) = 0$. Thus, the indices of all nodes in a period must sum to zero. Furthermore, since nodes with indices larger than 1 are only emergent [1], it follows that the nodes in a period must appear in pairs carrying the opposite signs, with or without a mirror symmetry.

The topological argument above shows that the nodes must always show up in pairs. However, it does not predict the existence or the location of the nodes. Thus, a microscopic theory is needed to understand the broadband binding of the nodes at $z = 0$. We note that $z = 0$ is a mirror plane of the structure but not the field, since the field is only incident from one side. (In fact, one can prove that a topological node can not exist on any mirror plane of the electromagnetic field.) In the following, we show that the broadband binding of the nodes is enforced by a combination of the mirror symmetry with respect to $z = 0$ and the time-reversal symmetry.

The intuition here is to examine the Fourier components of the electromagnetic fields, since a node can only form where the components cancel. Considering light incidence from the top, as a result of the Bloch theorem, we can decompose the field in the dielectric layer as

$$\begin{aligned} E(x, z) &= \sum_{n \geq 0} [\alpha_n(z) \cos(nGx) + \beta_n(z) \sin(nGx)] \\ &\doteq \sum_{n \geq 0} [f_n(x, z) + g_n(x, z)] \end{aligned} \tag{3}$$

where $\alpha_n(z)$ is a complex function, and n is an integer. Here we have assumed an incident wave amplitude of 1.

We now consider the time-reversed scenario, where the electric field becomes $E^*(x, z)$. The time-reversed scenario corresponds to having light incident from both sides: we take the time-reversal of the transmitted and reflected waves as inputs, and the output is the time-reversal of the original incident wave. Thus, denoting the transmission and reflection coefficients as t and r, we have

$$r^* E(x, z) + t^* E'(x, z) = E^*(x, z) \tag{4}$$

where $E'(x, z)$ is the field generated by an incident wave of amplitude 1 from the bottom. Due to the mirror symmetry at $z = 0$, $E'(x, z) = E(x, -z)$. Thus, at $z = 0$, we have

$$(r^* + t^*) = \frac{E^*(x, 0)}{E(x, 0)} \tag{5}$$

The left-hand side of Eq. (5) is independent of x. Thus, $E^*(x, 0)$ and $E(x, 0)$ only differ by a global phase factor independent of x. Since the global phase can be arbitrarily set by controlling the phase of the incident wave, it follows that $E(x, 0)$ can be chosen to be real everywhere on the z-mirror plane. As a result, all $f_n(x, 0)$ and $g_n(x, 0)$ must be real as well, i.e. they are either in-phase or 180° out-of-phase to each other. We emphasize that the argument here only requires the mirror symmetry with respect to $z = 0$, but not the mirror symmetry in x [23].

To understand the implication of this phase constraint, we consider the evolution of the nodes as a function of wavelength. In the long-wavelength limit, all Fourier components are negligibly small except for the lowest order, f_0. The field in the dielectric layer approaches a plane-wave shape where no topological node can be found. As the wavelength decreases, the next-lowest order f_1 or g_1 increases until their amplitude $|\alpha_1(0)|$ or $|\beta_1(0)|$ exceeds $|\alpha_0(0)|$, where the nodes are created on the $z = 0$ plane due to the phase constraint. Due to the mirror symmetry at $x = 0$ in the structure here, $g_1 = 0$. $|\alpha_1(0)|$ exceeds $|\alpha_0(0)|$ near the wavelength of $3L$ as is shown in Fig. 3, when two nodes are created at the $x = 0$ mirror plane. They then move away from $x = 0$ at shorter wavelengths, as can be observed in Fig. 1c-e. Once the nodes appear, they are confined at $z = 0$.

In fact, the binding at $z = 0$ is exact to arbitrary orders. Since all f_n and g_n are real at $z = 0$, the sum $(\sum_{n \geq 1} f_n + g_n)$ is still real, i.e. it is in-phase or 180° out-of-phase to f_0 at $z = 0$. Thus, as higher order $(n > 1)$ modes are excited at shorter wavelengths, e.g. at $1.25L$ in Fig. 1g, more topological nodes appear at exactly $z = 0$.

It should be noted that away from $z = 0$ the field components may still happen to cancel, where a node is formed. But those nodes are not bound to any special locations, and they generally move in a complex fashion
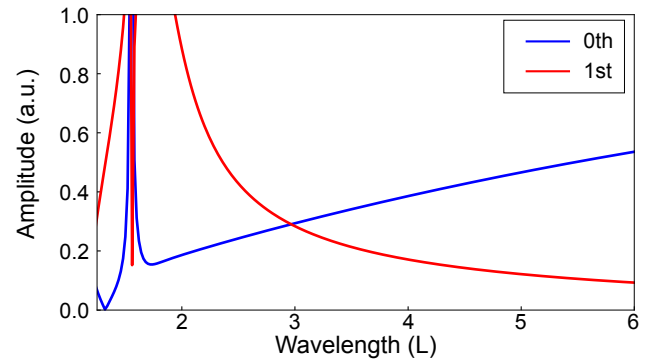

Figure 3. The amplitudes $|\alpha(0)|$ of the 0th (blue) and 1st (red) order Fourier components as a function of wavelength. As wavelength decreases, $|\alpha_1(0)|$ increases and exceeds $|\alpha_0(0)|$ near the wavelength of $3L$.
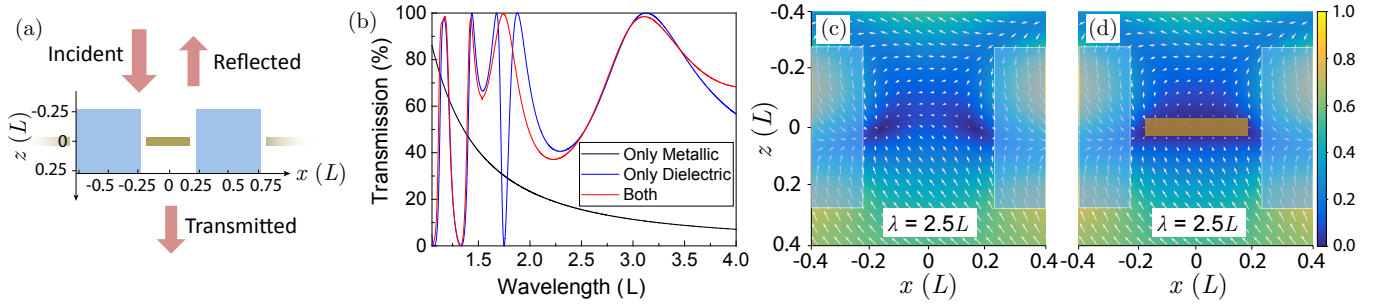
Figure 4. (a) A periodic array of dielectric (blue) and metallic (yellow) objects. The metallic objects have a permittivity of $\varepsilon_m = -3500 + 1467i$, and a size of $0.35 \times 0.05\,L$. (b) Transmission spectra with metallic objects only (black), dielectric objects only (blue), and both dielectric and metallic objects existing (red). (c) and (d), the field distribution at the wavelength of $2.5\,L$ with and without the metal objects as a comparison. The dielectric objects are indicated in the blue shading, while the metallic object is indicated in the yellow rectangle.

as wavelength changes.

The existence of the topological nodes at $z = 0$ does not depend on any resonances in the material or in the structure. In fact, the nodes will steer clear of a guided resonance. For example, there is a guided resonance at the wavelength of $1.75\,L$ in the structure (Fig. 1f) [27, 28]. Here, the electromagnetic field does not contain any topological node, rather it contains nodal lines which do not carry a topological index. On resonance, the field distribution can be well approximated by a standing wave pattern. A standing wave is time-reversal symmetric, thus it can not carry any topological nodes since a node flips its sign under time-reversal [23]. Furthermore, a standing wave is real up to a global phase. Therefore, the phasor vectors of a standing wave should be largely parallel to each other, as is observed in Fig. 1f. In general, we observe topological nodes and their binding to the $z = 0$ plane in a wide range of wavelengths away from the guided resonance.

Due to the broadband binding of multiple topological nodes at $z = 0$, the field distribution typically exhibits deep valleys at $z = 0$. As an implication, such valleys can be used to hide objects.

As a demonstration, we perform a set of simulations as is shown in Fig. 4, where we place a rectangular metallic object centered at the $z = 0$ plane. Fig. 4b shows the transmission spectra of 1) the dielectric layer, 2) the metallic object by itself, and 3) the combination of the metallic object with the dielectric layer. We observe that the transmission spectra of the dielectric layer with (red curve) or without (blue curve) the metallic object are very close to each other in the broad wavelength range of 1.1-3.5 L, except in a narrow region near $1.75\,L$ where the structure supports a guided resonance. As such, the metallic object is well hidden in the vicinity of the dielectric objects, even though the metallic object covers 35% of a period and the object by itself strongly scatters light, characterized by the low transmission (black curve) in Fig. 4b. As a visualization, we compare the field dis-

tribution with and without the metallic objects at the wavelength of $2.5\,L$ in Fig. 4c and d. It is clear that due to the topological nodes at $z = 0$, the added metallic object only represents a week perturbation to the electromagnetic field. As such, the metallic object is invisible in both the far field and the near field.

We note that the broadband hiding is independent of the detailed geometry of the metallic objects. Other shapes of objects can be hidden in the same dielectric structure as well [23]. We also note that the broadband hiding effect here is not simply because high-index materials tend to concentrate light away from the gap regions, since without the broadband binding of the topological nodes the metallic objects would typically not be in the field minimum over a broad wavelength range [23].

The hiding effect demonstrated here, which hides the added metallic objects in the vicinity of an existing dielectric structure, is different from the previously discussed cloaking effects that also apply to small objects [29–31]. Here, the existing dielectric environment generating the nodes is not necessarily invisible to external radiation. Such a hiding capability is important, for instance, when certain parts of an optical device need to be hidden to avoid any interference with the device's optical functionality. A typical example is the transparent electrode [32–34], where one embeds metallic wires in an optical device as contacts. The device itself, i.e. the dielectric parts, need to stay visible to perform optical functionalities such as light detection, light emission, or energy conversion. The electrodes however, need to be hidden to avoid any disturbance of the electromagnetic field. Furthermore, while the previously discussed cloaking effects typically exist in a narrow bandwidth, the hiding effect demonstrated here does not depend on any resonances, and allows broadband invisibility.

In summary, we have studied the topological nodes in electromagnetic fields. We show that it is possible to bind the location of the topological nodes to a specific plane using a combination of time-reversal symmetry and

mirror symmetry. Such binding does not rely on any resonances in the structure, and is robust over a wide wavelength range. As an implication, we demonstrate that the nodes can be used for hiding of metallic objects in a dielectric environment over a broadband wavelength range.

―――――――

* shanhui@stanford.edu

[1] M. R. Dennis, K. O'Holleran, and M. J. Padgett, in *Progress in Optics*, Vol. 53 (Elsevier B.V., 2009) pp. 293–363.

[2] J. F. Nye and M. V. Berry, Proceedings of the Royal Society A: Mathematical, Physical and Engineering Sciences **336**, 165 (1974).

[3] M. S. Soskin and M. V. Vasnetsov, Progress in optics **42**, 219 (2001).

[4] L. Allen, M. W. Beijersbergen, R. J. C. Spreeuw, and J. P. Woerdman, Physical Review A **45**, 8185 (1992).

[5] J. Ng, Z. Lin, and C. T. Chan, Physical Review Letters **104**, 103601 (2010).

[6] N. Yu, P. Genevet, M. A. Kats, F. Aieta, J.-P. Tetienne, F. Capasso, and Z. Gaburro, Science **334**, 333 (2011).

[7] M. R. Dennis and J. B. Götte, Physical Review Letters **109**, 183903 (2012).

[8] J. Wang, J.-Y. Yang, I. M. Fazal, N. Ahmed, Y. Yan, H. Huang, Y. Ren, Y. Yue, S. Dolinar, M. Tur, and A. E. Willner, Nature Photonics **6**, 488 (2012).

[9] X. Cai, J. Wang, M. J. Strain, B. Johnson-Morris, J. Zhu, M. Sorel, J. L. O'Brien, M. G. Thompson, and S. Yu, Science **338**, 363 (2012).

[10] J. Sun, J. Zeng, X. Wang, A. N. Cartwright, and N. M. Litchinitser, Scientific Reports **4**, 2 (2014).

[11] X. Ma, M. Pu, X. Li, C. Huang, Y. Wang, W. Pan, B. Zhao, J. Cui, C. Wang, Z. Zhao, and X. Luo, Scientific Reports **5**, 10365 (2015).

[12] M. R. Dennis, R. P. King, B. Jack, K. O'Holleran, and M. J. Padgett, Nature Physics **6**, 118 (2010).

[13] M. V. Berry and M. R. Dennis, Proceedings of the Royal Society A: Mathematical, Physical and Engineering Sciences **456**, 2059 (2000).

[14] W. Wang, S. G. Hanson, Y. Miyamoto, and M. Takeda, Physical Review Letters **94**, 103902 (2005).

[15] M. V. Berry, Philosophical Transactions: Mathematical, Physical and Engineering Sciences **360**, 1023 (2002).

[16] N. Shvartsman and I. Freund, Physical Review Letters **72**, 1008 (1994).

[17] V. Liu and S. Fan, Computer Physics Communications **183**, 2233 (2012).

[18] D. M. Whittaker and I. S. Culshaw, Physical Review B **60**, 2610 (1999).

[19] M. Liscidini, D. Gerace, L. C. Andreani, and J. E. Sipe, Physical Review B **77**, 035324 (2008).

[20] John Willard Milnor, *Topology From the differentiable point of view* (Princeton University Press, 1997).

[21] P. A. Firby and C. F. Gardiner, *Surface topology* (Ellis Horwood, 1991).

[22] B. Zhen, C. W. Hsu, L. Lu, A. D. Stone, and M. Soljačić, Physical Review Letters **113**, 257401 (2014).

[23] Please see supplementary for further illustration.

[24] A. Kosinksi, *Differential manifolds* (Academic Press, 1993).

[25] H. Hopf, Mathematische Annalen **96**, 225 (1927).

[26] C. C. Pugh, Topology **7**, 217 (1968).

[27] S. S. Wang, R. Magnusson, J. S. Bagby, and M. G. Moharam, Journal of the Optical Society of America A **7**, 1470 (1990).

[28] S. Fan and J. D. Joannopoulos, Physical Review B **65**, 235112 (2002).

[29] R. Fleury, F. Monticone, and A. Alù, Physical Review Applied **4**, 037001 (2015).

[30] A. Alù and N. Engheta, Physical Review Letters **100**, 113901 (2008).

[31] M. Xiao, X. Huang, J.-W. Dong, and C. T. Chan, Optics letters **37**, 4594 (2012).

[32] A. Khan, S. Lee, T. Jang, Z. Xiong, C. Zhang, J. Tang, L. J. Guo, and L. Wen-Di, Small **12**, 3021 (2016).

[33] K. Ellmer, Nature Photonics **6**, 809 (2012).

[34] H. Wu, D. Kong, Z. Ruan, P.-C. Hsu, S. Wang, Z. Yu, T. J. Carney, L. Hu, S. Fan, and Y. Cui, Nature Nanotechnology **8**, 421 (2013).